4-2020

Inelastic Behavior and Seismic Design of Multistory Chevron-Braced Frames with Yielding Beams

Charles W. Roeder
University of Washington

Andrew D. Sen
Marquette University, andrew.sen@marquette.edu

Hayato Asada
Kobe University

Sara M. Ibarra
University of Washington - Seattle

Dawn E. Lehman
University of Washington

See next page for additional authors

Journal of Constructional Steel Research, Vol. 167 (April 2020): 105817. DOI.

Inelastic Behavior and Seismic Design of Multistory Chevron-Braced Frames with Yielding Beams

Charles W. Roeder
Department of Civil and Environmental Engineering, University of Washington, Seattle, WA
Andrew D. Sen
Department of Civil and Environmental Engineering, University of Washington, Seattle, WA
Hayato Asada
Department of Architecture, Kobe University, Kobe, Japan
Sara M.Ibarra
Department of Civil and Environmental Engineering, University of Washington, Seattle, WA
Dawn E. Lehman
Department of Civil and Environmental Engineering, University of Washington, Seattle, WA
Jeffrey W. Berman
Department of Civil and Environmental Engineering, University of Washington, Seattle, WA

Keh-Chyuan Tsai
Department of Civil Engineering, National Taiwan University, Taipei, Taiwan
Ching-Yi Tsai
Department of Civil Engineering, National Taiwan University, Taipei, Taiwan
An-Chien Wu
National Center for Research on Earthquake Engineering, Taipei, Taiwan
Kung-Juin Wang
National Center for Research on Earthquake Engineering, Taipei, Taiwan
Ruyue Liu
Department of Civil Engineering, Xi'an Universotu of Architecture and Technology, Xi'an, China

Abstract

Chevron or inverted V-braced frames offer numerous architectural and structural advantages, but the current special concentrically braced frame (SCBF) seismic-design requirements in the American Institute of Steel Construction (AISC) *Seismic Provisions for Structural Steel Buildings* lead to deep, heavy chevron beams; as a result, few chevron SCBFs are built today. Recent research on single-story chevron SCBFs demonstrated that beam yielding can be advantageous at higher demand levels, and design for large, inelastic unbalanced brace-force demands may still result in acceptable seismic performance. However, this prior research did not consider the response of multistory frames. In particular, questions remain as to the potential for concentration of damage, the impacts of composite slabs, and the effects of different beam-to-column connections; these issues can only be investigated using multistory frames. A companion research program was conducted to investigate multistory systems with chevron SCBFs using experimental and computational simulation methods. In the first phase of the research, a three-story chevron SCBF designed to permit beam yielding was tested at the National Center for Research on Earthquake Engineering (NCREE) Laboratory in Taipei, Taiwan. The test results were then used to validate a nonlinear, continuum finite-element model. A limited parametric study was conducted to build upon and further the experiments, specifically to evaluate different beam strengths and stiffnesses. These results were combined to develop design recommendations for chevron SCBFs with yielding beams.

Keywords

Braced frames, Steel, Chevron, Seismic, Inelastic behavior, Full-scale testing, Finite-element modeling

1. Introduction

Historically, chevron (V- or inverted V-braced) concentrically braced frames (CBFs) were a preferred structural system for seismic design because they offer excellent strength and stiffness and numerous architectural advantages, most importantly permitting openings such as windows and doors within the lateral-load-resisting system (LLRS). In fact, most of the CBFs built prior to 1988 employed chevron CBFs for part or all of the LLRS. In 1988, the first capacity-based design requirements were introduced in US code [1]. Then, in 1997, the first edition of the American Institute of Steel Construction (AISC) *Seismic Provisions for Structural Steel Buildings* [2] expanded these capacity-based design requirements, which are very similar to those in the current (2016) AISC *Seismic Provisions* for special CBFs (SCBFs) [3]. This current seismic specification in the US requires that:

- Braces are designed to resist the factored design lateral loads while meeting global ($L_c/r = KL/r$) and local slenderness (width-to-thickness ratio, or b/t in rectangular HSS braces) limits;
- Connections, beams, and columns are designed to develop the expected tensile ($P_{ye} = R_y F_y A_g$), compressive ($P_{cre} = 1.14 F_{cre} A_g$), and post-buckling deteriorated resistance ($0.3 P_{cre}$) of the braces,

where P_{cre} is the expected compressive capacity of the brace, P_{ye} is the expected tensile capacity of the brace, R_y is the material-specific overstrength factor, F_y is the yield stress of the brace material, F_{cre} is the critical stress at buckling evaluated with R_yF_y, and A_g is the gross area of the brace;

- Beam-column connections are designed to either assure adequate connection rotation or development of the full plastic capacity of the beam;
- Gusset plates are designed to accommodate end rotation of the brace and sustain the expected capacity of the brace; and
- Demand critical welds are used in regions where yielding is expected.

Chevron CBFs (see Fig. 1) use a pair of braces in each bay; under lateral loading, one brace is in compression and the other is in tension. The beam supporting the chevron braces (herein referred to as the chevron beam) is currently designed under two loading states: one in which the expected resistances of the braces (P_{ye} and P_{cre}) are developed and another in which the resistance of the compressive brace has deteriorated due to a large post-buckling deformation (P_{ye} and $0.3P_{cre}$). This latter state induces significant axial load and large bending moment in the chevron beam, which requires deep, heavy beams. These stringent chevron-beam requirements were founded on experimental research in the 1980s [[4], [5], [6]], but the tested beam and brace connection details differ significantly from those used in current practice. However, more recently, large-scale experimental testing of older CBFs [7,8] and a modern "R = 3" CBF [9] demonstrated that chevron beams which did not meet these requirements are not necessarily detrimental to nonlinear response.

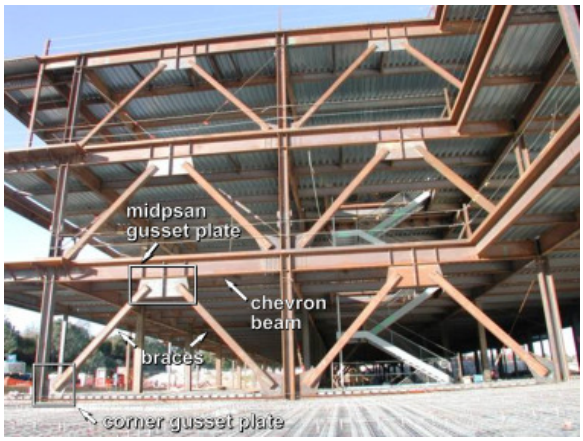

Fig. 1. Chevron SCBF with me (Courtesy of AISC).

To further study the impact and potential benefits of chevron beams permitted to yield under moderate-to-large drift demands, Roeder et al. [10] experimentally and analytically investigated the inelastic seismic performance of single-story chevron CBFs. The tests were designed as SCBFs in all aspects except for the beam-strength requirement, and hence these specimens are referred to as SCBFs. Six large-scale single-story chevron SCBFs were tested with different beam strengths and stiffnesses. The tests demonstrated that beam yielding is beneficial to the nonlinear behavior and results in significantly larger story drifts prior to brace fracture than SCBFs with other configurations and chevron SCBFs with elastic beams. This limited yielding of the chevron beam and its associated vertical deflection increases the compressive deformation demands but decreases the tensile deformation demands on the braces. This latter behavior, which is also influenced by chevron beam stiffness [[11], [12], [13]], reduces the low-cycle tensile strain demands and therefore prolongs brace fracture life.

The strength of the beam relative to the braces cannot be completely disregarded, however, when high system ductility demand is expected. The reduced tensile deformation demand in the braces with beam yielding and

vertical deflection results in reduced frame resistance. Even so, this reduction can be small, even for a fairly significant reduction in beam size compared to that required with current design provisions. Further, it is possible that beam deflection (and hence rotation demands in connections or plastic hinges) can be excessive. Thus, ensuring the strength of the LLRS does not fall below the design forces and limiting vertical beam deflection are two proposed criteria that guide beam design. The single-story chevron tests suggested that this lower-bound limit on the beam resistance should be in the range of 25–33% of the current beam-strength requirement for the configuration and braces tested.

Nonlinear analytical models were validated using these experimental results and then were used to further the experimental research. These analyses, combined with the experimental observations, led to the following conclusions:

1) The maximum lateral resistance of the frame decreases with increased beam yielding, but the change in lateral resistance is smaller than the reduction in beam resistance. The lateral resistance remains larger than the design lateral resistance through large inelastic deformation if the beam strength is larger than approximately 30% of the current SCBF requirement.
2) Braces buckle in compression regardless of beam strength, and degradation in compressive brace force is similar regardless of the beam strength. However, the maximum tensile brace force approaches the magnitude of the brace buckling force with weak chevron beams.
3) There are two design load states, shown in Fig. 2, that must be considered in design of the chevron beam, including the combination of the expected brace forces at incipient buckling (Fig. 2a) and the degraded tensile and compressive capacity (Fig. 2b). These load states differ from those required in the current (2016) AISC *Seismic Provisions* because the tension brace force is equal in magnitude to the expected compressive strength here. Further, the prior experimental and numerical results suggest the chevron SCBF behavior will be influenced by axial yielding of chevron beams if the beam strength is less than about 25% of current SCBF requirements, suggesting a lower bound for design.

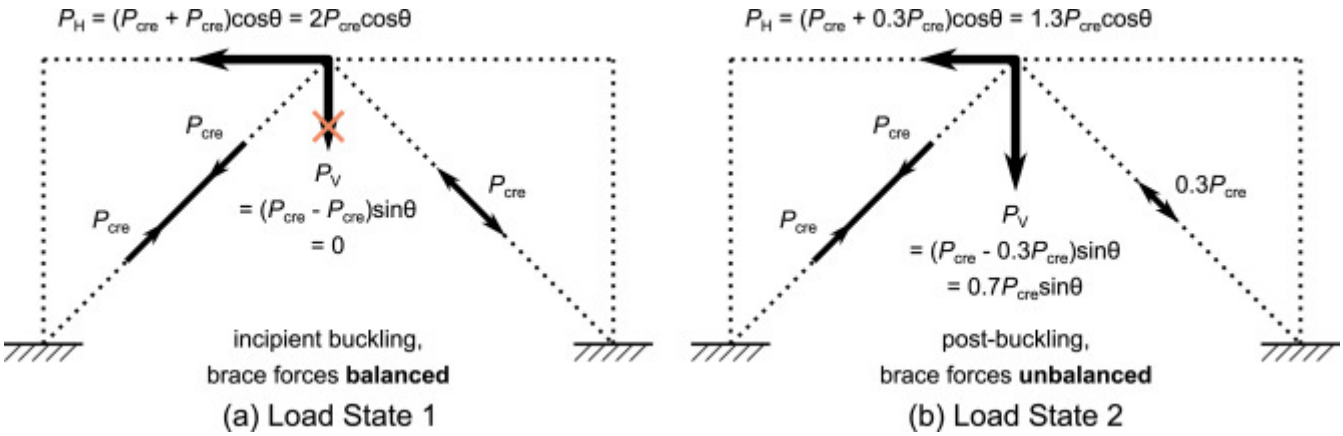

Fig. 2. Proposed design load states for yielding chevron beams in SCBFs.

This prior research was beneficial to understanding and founding a new class of chevron SCBF system. However, there were several limitations to the work. First, the specimens did not have a composite floor slab, and the contributions of the composite slab in resisting the demands, in particular the horizontal component of the brace forces, are not known. Second, multistory chevron braced frames have corner gusset plates at every beam-column connection, but the single-story test frames used simple shear-plate beam-to-column connections; the impact of the rotational resistance of these gusset plates should be investigated. Third, SCBFs

have a potential for concentrating inelastic deformation into a single story of the frame, and engineers have expressed concern that yielding chevron beams may increase this potential for concentrated damage [14,15]; this response mechanism can only be studied using multistory frames. Finally, while the single-story chevron research showed a potential range for acceptable beam strength, uncertainty remains as to the minimum beam size when the above issues are considered.

To understand these additional uncertainties and develop a design expression for multistory chevron SCBFs, a second phase of the research was conducted to specifically investigate multistory chevron braced frames with beam yielding. This phase consisted of three primary components: (1) a large-scale experimental investigation of a three-story chevron SCBF with yielding beams, (2) a finite-element analysis study to validate a modeling approach using the test specimen, and (3) a finite-element analysis parametric study on the effects of beam strength. Research results and proposed design expressions for both incipient and post-buckling load states that permit controlled chevron-beam yielding are provided here.

2. Experimental investigation

2.1. Experimental program

2.1.1. Specimen design

A three-story chevron SCBF with the proposed yielding-beam mechanism was tested at the National Center for Research on Earthquake Engineering (NCREE) Laboratory in Taipei, Taiwan, with funding provided by the American Institute of Steel Construction. Fig. 3a shows a photograph of the test frame and setup, and all primary member sizes are indicated in Fig. 3b. All structural members are US designations, but all dimensions are in SI units. To minimize the cost of the test, the frame was designed and built to utilize a test setup developed for prior three-story SCBF tests [16]. The frame was tested in a vertical position with lateral loads applied by actuators loading the frame through the top story slab. Consequently, each story was subjected to the same story shear and utilized the same brace section. The braces were sized to be the largest braces that conservatively developed the full frame lateral resistance with the chosen actuators. The overall geometry of the frame was nearly identical to that used in the prior research. The braces were HSS5 × 5 × 1/2 and met the ASTM A1085 specification.

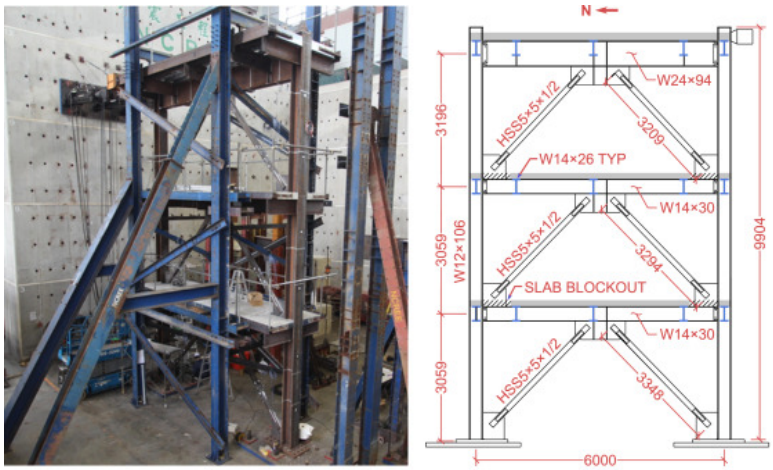

(a) Photograph of test frame and setup (Note: blue members comprise the out-of-plane restarint frame)

(b) Elevation drawing of test frame (all units mm)

Fig. 3. Three-story test frame. (For interpretation of the references to colour in this figure legend, the reader is referred to the Web version of this article.)

A W14 × 30 beam was used for the bottom two floor levels. This beam has approximately 34% of the resistance required by the unbalanced load requirement of the 2016 AISC *Seismic Provisions* at the time of testing [3], which is at or near the limit on permissible beam yielding from the single-story chevron research [10]. This relative strength was targeted in the beam design to investigate the boundary of acceptable response with the yielding beam mechanism. To compute the beam strength, it was assumed that: (1) the beam develops plastic hinges at the edge of both the corner and midspan gusset plates, (2) composite action does not contribute to beam resistance, and (3) the axial force in the beam from the unbalanced brace forces is distributed equally to either side of the beam. Due to the role of the top slab in transferring force to the test frame, vertical deflection could not be tolerated in this beam since this could result in damage to the actuators and other equipment. As a result, the top beam was designed to remain elastic under all conditions and was a W24 × 94 section. The columns were designed to resist a nominal gravity load and the maximum expected brace forces, as required by the current (2016) AISC *Seismic Provisions* for SCBFs, resulting in W12 × 106 sections. Note that the maximum expected brace forces would develop approximately 50% of the nominal strength of the columns in compression. All beams and columns were ASTM A992 steel.

A 75-mm-on-75-mm composite slab was used on the first and second stories. Concrete was blocked out around corner gussets to permit end rotation of the braces. Normal-weight concrete was used and 19-mm (0.75 in.) shear studs were spaced at 305 mm (12 in.) to achieve partial (approximately 20%) composite action. The slab thickness and shear-stud spacing was designed to represent common composite beam design practice in the US. Steel edge beams were placed over a short segment of these beam spans, but the edge beams did not span the full length to avoid restraining vertical deflection. The metal deck was oriented with ribs parallel to the W14 × 30 beams and supported by transverse W14 × 26 beam stubs.

The top slab was 125-mm thick over the same metal deck (i.e., 200 mm total thickness) with steel-fiber-reinforced concrete and steel edge beams along the entire length. The top slab was thicker, stiffer, and stronger, with two 19-mm (0.75-in.) shear studs spaced at 150 mm (6 in.). It is noted that the edge beams here were continuous in order to ensure force transfer. The design of the top beam and slab had adverse effects on the test, as will be discussed later.

The corner and midspan gusset plates at every story were designed using the balanced design procedure (BDP) to enhance the deformation capacity of the brace-gusset plate subassmeblage [17]. This method employs an $8t_p$ elliptical clearance at the corner gusset plates and a $6t_p$ linear offset at the midspan gusset plates. Further, the BDP permits limited yielding of the gusset plates in tension using relaxed block shear requirements and a 37-degree Whitmore width angle (a variation to the BDP discussed in Sen et al. [18]), resulting in smaller, more compact gusset plate designs.

Fig. 4 shows typical connection details of the test frame. Various beam-to-column connections were considered, but welded flange-welded web connections were used for all beam-to-column connections based on preliminary Abaqus [19] analyses and the recommendations of an advisory panel of structural engineering practitioners. As shown in Fig. 4b, the columns were welded to base plates using complete joint penetration welds. The base plates were attached to larger anchor plates using a dense array of anchor rods, providing full rotational restraint at the base and significantly increasing the stiffness of the first story. Due to this fixity, the columns were expected to yield at the base and modestly contribute to the frame resistance.

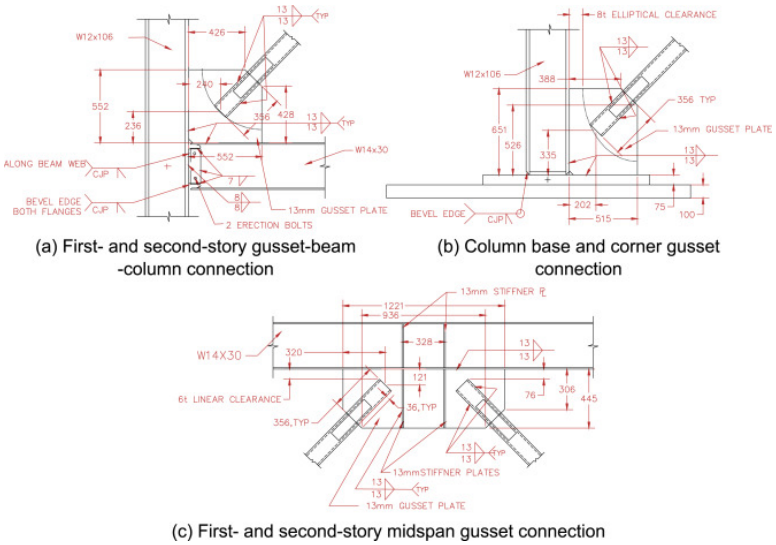

Fig. 4. Typical connection details for test frame.

Table 1 provides the measured material yield and ultimate tensile strengths, F_y and F_u, along with the ratios of measured-to-nominal strengths of the structural sections and plates. The wide flange sections used for the beams and columns were A992 steel and the braces were A1085 steel; these members were shipped to Taiwan from the US. The measured yield stresses of the W14 × 30, W24 × 94, and HSS5 × 5 × 1/2 were all somewhat larger than those suggested by the 2016 AISC *Seismic Provisions* (i.e., R_yF_y), but it is noted that this overstrength did not have an appreciable effect on the findings herein. The gusset plates and stiffeners were Taiwanese steel selected to closely match A572 Grade 50 material. The compressive strength of the concrete in the floor slabs was measured as 38 MPa (5.5 ksi) for the bottom two levels and 36 MPa (5.2 ksi) on top level on the day of the test.

Table 1. Steel measured material properties.

Section	**Specification**	F_y		F_u		$F_y/F_{y,nom}$	$F_u/F_{u,nom}$
		(MPa)	**(ksi)**	**(MPa)**	**(ksi)**		
W14 × 30	A992 Gr. 50	385	55.8	510	74.0	1.12	1.14
W12 × 106	A992 Gr. 50	379	55.0	521	75.6	1.10	1.16
W24 × 94	A992 Gr. 50	416	60.4	534	77.5	1.21	1.19
HSS5 × 5 × 1/2	A1085	490	71.0	552	80.1	1.42	1.23
13-mm plate	SN490B	390	56.5	532	77.2	1.20	1.19
10-mm plate	SN490B	370	53.6	534	77.4	1.14	1.19

2.1.2. Test setup

An out-of-plane (OOP) support frame (see Fig. 3a) controlled OOP movement and ensured lateral stability of the frame. The first- and second-story beams and slabs were restrained against lateral movements by the OOP support frame at the chevron beam quarter points. The ends of the transverse beams had two points of contact with the OOP frame which resisted rotation of the slab and torsion of the chevron beam at the quarter points. The concrete slab was expected to provide lateral support to other sections of the chevron beams. This arrangement was necessary to accommodate the large vertical deflections at midspan of the beam with yielding chevron beams but resulted in reduced restraint to chevron beam lateral and torsional deformations. The top slab had rotational and lateral restraint over its entire length, and in contrast to the lower stories, provided significantly more restraint than in an actual building; this additional restraint resulted in local damage as discussed below (this damage did not impact the performance of the system). Rotational restraint at the top

was provided by rollers, which were supported by the OOP support frame and prevented differential vertical movement of the top slab.

The force from the actuators was transferred through transfer beams to two continuous edge beams with shear studs along the length of the third-story floor slab. Then, the force was transferred from the slab to the top chevron beam through closely spaced shear studs, as described above. The three (3) actuators, located on the south side of the frame, acted in compression with positive deflections to the north and in tension when the frame had negative deflections to the south. The center actuator was controlled by a displacement protocol (see Fig. 5), and the east and west actuators were constrained to match the displacement of the center actuator.

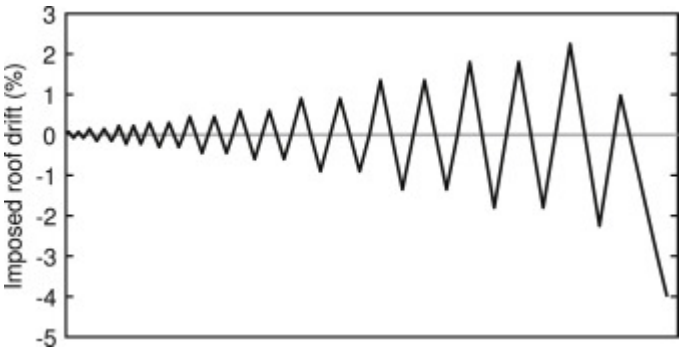

Fig. 5. Roof drift loading protocol.

The displacement protocol controlled the roof drift and was based upon the protocol used for prior single-story chevron SCBF tests, which was developed to capture the initiation of brace buckling (and potentially brace yielding) while retaining the objective of ATC-24 [20]. A Temposonic linear variable displacement transducer (LVDT) aligned with the center of the top slab at the north column flange was used to control the displacement. The protocol was based on a yield drift, Δ_y, taken as the drift at brace buckling, which was estimated to be 29 mm (0.3% drift) from preliminary analyses. The specimen was subjected to two cycles at each target displacement with the exception of the final half cycle. Each target displacement was set as a multiple of the yield displacement. Two variations to the specified protocol were made: (1) small elastic cycles were completed to verify operation of the instrumentation prior to application of this displacement protocol and (2) the protocol was adjusted in the penultimate half-cycle to accommodate changes after initial fracture in the test specimen. Since the stiffness of the three stories varied due to differences in beam-to-column connections (i.e., adjacency of gusset plates), the column bases, and the third-story beam size, the drift was not distributed evenly along the height of the building and the individual story drifts differ from the average (i.e., roof) drift.

2.1.3. Instrumentation

Instrumentation was installed to monitor local and global deformations as well as movement of the specimen. A summary is provided here, and additional information can be found in Ibarra [21]. Strain gauges were used to monitor regions of the braces, beams, and columns in regions expected to remain elastic; after testing the strains elastic modulus were used to calculate member force and bending-moment demands. LVDTs were used to measure midspan deflection of the beams, OOP rotation of the gusset plates, and lateral deflection of the top level of the structure. String potentiometers were used to measure lateral displacement of the lower two floors, elongation and shortening of the braces, and some OOP movements of the gusset plates. Inclinometers were attached to beams, columns and slabs to measure rotations at various locations.

Two optical data acquisition systems were used measure local deformations and to duplicate and verify other global electronic measurements. Northern Digital Inc. (NDI) Optotrak cameras and light-emitting diodes (LEDs)

were used to measure three-dimensional movements of the midspan gusset plate and portions of the beams and braces for the bottom story level. A NaturalPoint Inc. OptiTrack measurement system was used to collect similar measurements on the second floor. The latter optical system offered advantages in that it provided a longer range and wider monitoring volume, but its unique data structure limited opportunities to combine these data with other measurements. Load cells measured applied actuator loads, and dial gauges measured any inadvertent support movement. Whitewash was applied to hot rolled shapes where yielding was expected to visually document initiation and progression of yielding. Details about individual instruments and other aspects of the test setup can be found in the reference reports [21,22].

2.2. Experimental results

The test was completed on March 17, 2018. Fig. 6 shows the shear force as a function of the roof drift (roof displacement normalized by the height from the column base to the center of the actuators) as well as the force as a function of the individual story drifts. The shear force was the same for all three story levels throughout the test, but the story drift varied between stories because the top level was stiffer and stronger for the reasons discussed earlier. The expected lateral resistance of the frame, $2P_{cre}\cos\theta$, is noted on each plot, where P_{cre} is the expected compressive (i.e., buckling) strength of the braces based upon their actual lengths and the measured yield stress of the steel and θ is the inclination angle of the braces with respect to the horizontal.

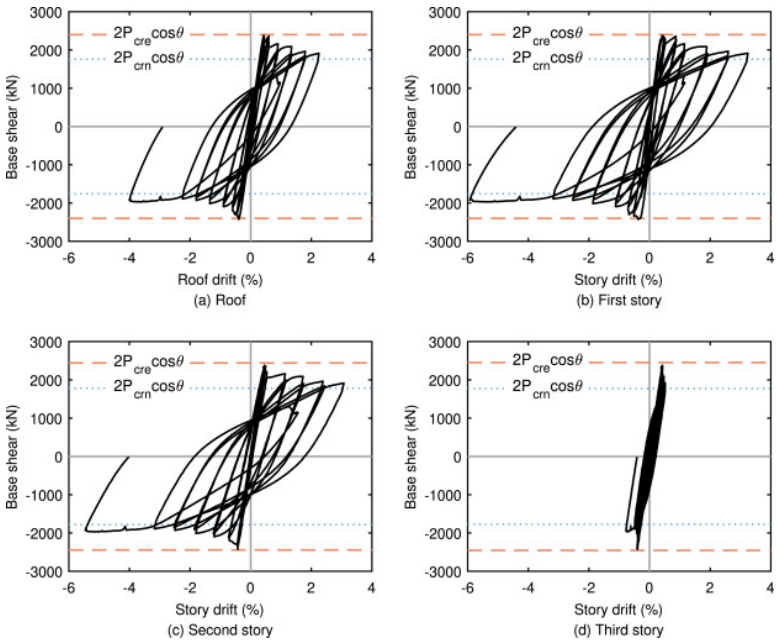

Fig. 6. Shear force versus drift plots.

At initiation of buckling, the tensile and compressive brace have approximately the same force. After brace buckling, the compressive force will decrease while the tensile brace force may continue to increase. Hence, $2P_{cre}\cos\theta$, is the expected design resistance. However, the design lateral resistance of the frame is based on the nominal brace capacity, P_{crn}, which is determined from the nominal yield stress and does not include the 1.14 (or 1/0.877) factor which discounts the initial out-of-straightness of the member. The design lateral resistance, $2P_{crn}\cos\theta$, is also shown on the plots in Fig. 6. This is the minimum capacity required from the SCBFs; frames that do not reach this strength do not have adequate capacity to resist the design loads and therefore would not be a valid design solution. This same criterion was used for the one-story frames, and the lowest beam size calculated using the results from those tests and analyses was used in this test. As such, the test was expected to reach the design strength but not significantly exceed it. This intention was supported by the results, as indicated in the figure.

The following provides an overview of the progression of response, yielding, and damage during testing of the three-story chevron SCBF:

- The initial elastic cycles of the test proceeded normally with lateral story drift relatively uniformly distributed over the three (3) stories of the frame. Initial brace buckling occurred in the bottom story of the frame at a story drift level of approximately 0.4% (see Fig. 7). Buckling of the second-story braces occurred at a slightly larger roof drift level but similar story drift level. The first-story braces buckled in the same OOP direction, but the second story braces buckled in opposite directions.

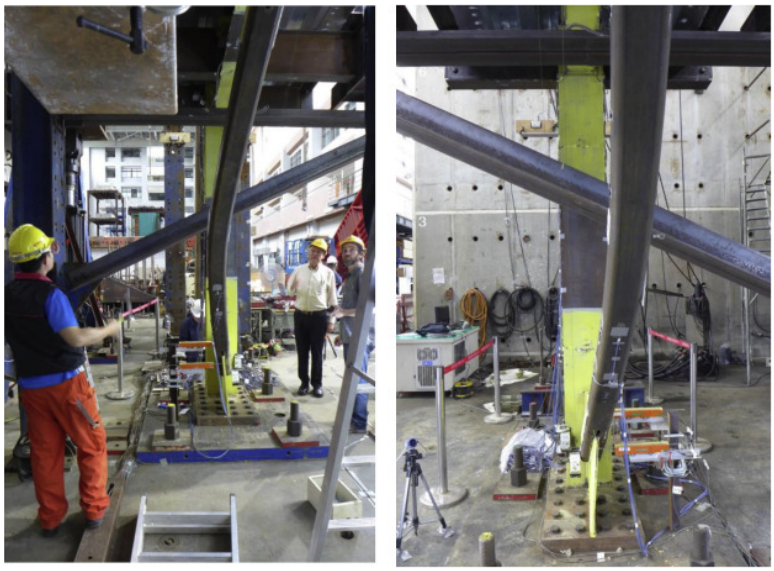

Fig. 7. Brace buckling of (a) north and (b) south brace at story drifts of +0.3% and −0.4%.

- The frame developed the expected lateral resistance ($2P_{cre}\cos\theta$) during these smaller deformation cycles, but this peak strength deteriorated at larger drift levels. The frame's absolute maximum lateral resistance was 2425 kN (544.9 kip). With increasing deformation, the inelastic deformation was approximately evenly distributed between the first and second stories, but the third story remained nearly elastic (as expected). The bottom two beams developed plastic hinges at the edges of the corner and midspan gusset plates, but the location of plastic hinging changed from one end to the other with reversal of the cyclic deformation. As brace out-of-plane deformation increased, significant yielding in the gusset plates of the bottom two stories was noted.
- Local buckling occurred at the beam plastic-hinge locations. Severe yielding and local buckling of the beam web and flange was noted at the plastic hinges adjacent to the corner gusset plates (see photos in Fig. 8, Fig. 9c). The extent of yielding and local buckling at plastic hinges adjacent to the midspan gusset plates was significantly smaller than at the corner gussets (compare Fig. 8a and c to Fig. 8b and d).

(a) South end of first-story beam at 2% story drift

(b) Midspan gusset and first-story beam at 2% story drift

(c) North end of first-story beam at 3% story drift

(d) Midspan gusset and first-story beam at 3% story drift

Fig. 8. Yielding and buckling of beam and gusset plates at different story-drift levels.

(a) Crack initiated at backing bar through the flange

(b) Crack progression through column web

Fig. 9. Photographs of fractured column.

- As brace buckling deformation increased, the bottom two beams twisted about their longitudinal axis within the unrestrained section of the floor. As a result, the beam and slab accommodated part of the rotation associated with brace buckling rather than being solely accommodated by deformation and rotation of the midspan gusset plate. This twisting increased the plastic deformation of the hinged locations in the beam near the corner gusset plates and decreased plastic deformation and local buckling at midspan gusset plates.
- Visible separation of the composite slab from the first-story beam was noted at 1.8% first-story drift. Separation of the slab from the transverse beam stubs was also apparent at larger drifts. Cracks in the slab were concentrated at each end of the slab and near the blockout. This is reasonable since the edge beams transferring the force to the slab ended just past the blockout, where the first beam shear studs were located.
- The frame sustained cyclic loading for nineteen full cycles before the inner flange of the second-story south column fractured at the bottom flange of the beam-to-column connection CJP weld. The crack originated behind the backing bar that was left in place. The fracture occurred as the frame was pushed in the north direction (positive drift movement). Upon fracture, the frame sustained a 30% loss in resistance in the positive loading direction but remained stable. The frame was inspected and deemed sufficiently stable to load in the negative-drift direction. This fracture resulted from the boundary conditions of the test, which were necessary to transfer the load from the actuator to the specimen and would not occur in an actual building.
- The frame deformed to a maximum average story drift of −4%, with corresponding first- and second-story drifts of −5.9% and −5.4%, respectively. As the frame was pushed south, the gap at the column

flange fracture closed. Despite the very large story drifts in the bottom two stories, none of the braces fractured. However, local cupping that precedes fracture of rectangular HSS braces was visible at the end of the test, indicating incipient fracture. The total drift ranges were 9.1% for the first story and 8.6% for the second story. Separation between the concrete slab and the steel beam was not observed for the top chevron beam but was very significant in the bottom two stories. Ten shear studs had pulled out of the first-story slab and 8 pulled out of the second-story slab due to this separation.

- Significant flexural yielding of the columns was noted adjacent to the first-story corner gusset plates, where the base plates provided full rotational restraint. There were no severe local deformations in the columns in this region.

2.2.1. Beam deflections

The vertical deflections of the beams for the bottom two stories are shown in Fig. 10. The figure shows that both beams had a maximum deflection of approximately 100 mm (4 inches) at 3% story drift, but the first-story beam deflection was slightly larger than that of the second-story beam. The maximum residual vertical beam displacement after the structure had sustained 3% story drift and lateral loads were removed were approximately 89 and 73 mm (3.5 and 2.9 inches) for the first and second stories, respectively (the 3% story-drift cycle was the last full cycle and the remainder of the loading subjected the structure to 6% story drift in the negative-displacement direction only). The clear beam span from face-to-face of the column was 5.67 m (18.6 ft), and so the maximum residual deflection was approximately 1/62. It is postulated that a deflection of this magnitude could be repaired to satisfy architectural requirements. However, larger story drifts and beam deflections are possible with actual earthquake loading which is not necessarily symmetric (especially, for example, with near-fault ground motions). In addition, this level of drift demand would not be expected in a moderate earthquake and hence would be relatively unlikely in the life of the building.

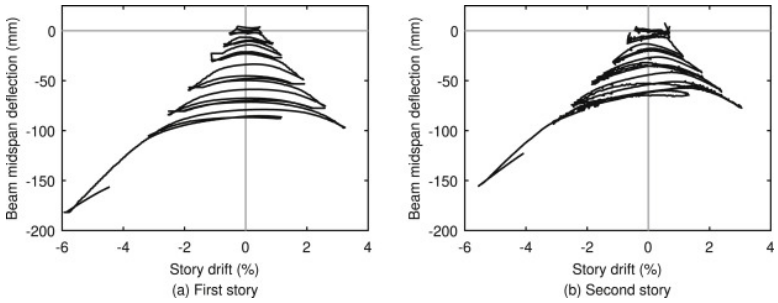

Fig. 10. Midspan deflection of chevron beams.

2.2.2. Story-drift distribution

The experimental results do not show concentration of damage in a single story, which has been attributed to chevron SCBFs. Note that all stories were designed with the same braces and loaded with the same shear force, and the bottom two stories had very similar inelastic deformation demands.

The top story had significantly smaller inelastic deformation, which was expected because this floor was designed to be significantly stiffer and stronger, as discussed earlier. Further, the top composite floor slab was thicker, had steel-fiber reinforcement, and contained approximately five times the total number of shear studs used in the lower floors. Thus, composite action contributed much more to the strength and stiffness of the top story, and very little yielding was noted. Buckling of the top story braces appears to have initiated but did not significantly contribute to frame deformation, as this occurred well after the lower story braces buckled.

2.2.3. Brace behavior

Fig. 11 shows brace axial force normalized by the absolute value of the predicted buckling force considering measured material properties, P_{cre}, plotted against the measured axial deformation normalized by the brace length in the bottom two stories of the frame. As described previously, brace axial force was computed using strain gauges placed on the braces in regions that largely remained elastic. When yielding did occur in the instrumented regions, a simple bilinear constitutive model was assumed to derive the stress from the recorded strain history. The responses of the top-story braces are not shown because they had insignificant inelastic deformation.

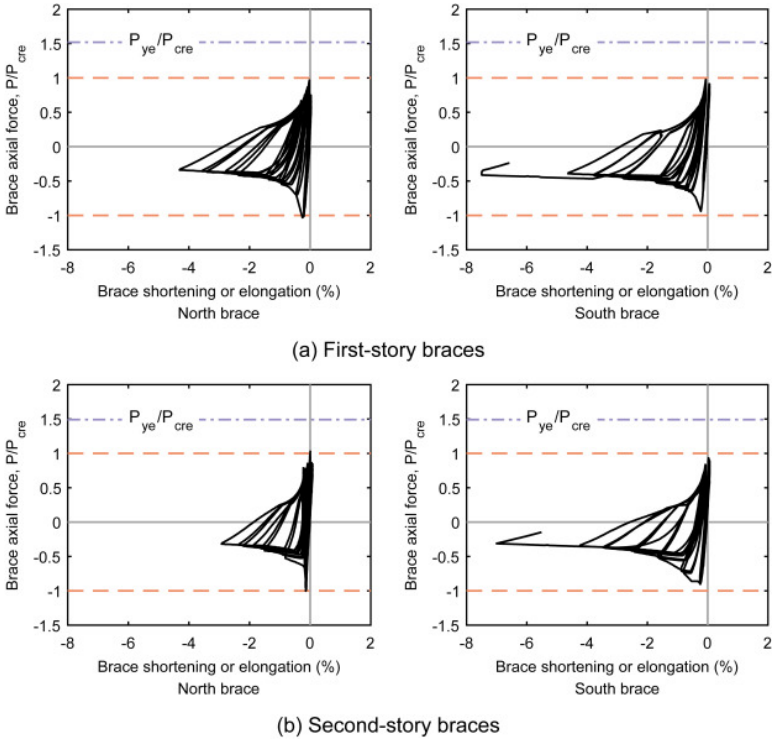

Fig. 11. Brace axial force versus axial deformation plots.

The braces in the bottom two stories sustained large axial shortening deformation but relatively smaller tensile elongation. This is the primary reason that chevron SCBFs with yielding beams develop larger inelastic deformations than other brace configurations prior to brace fracture (and consequently a reduction in low-cycle fatigue demands on the tension side of the response). The tensile yielding in these braces was limited and localized, associated with partial straightening of the buckled braces or from the plastic hinge that develops at the middle of brace at large OOP displacements. The reduction in the inelastic tensile strains delays fracture and increases the drift capacity of this system relative to other SCBF configurations. The braces of the bottom story sustained significant post-buckling deterioration of compressive resistance, but they retained 30–40% of their compressive capacity even at axial shortening of larger than 6%.

While all of the braces reached or slightly exceeded their compressive buckling load, none of the braces developed their expected tensile yield force, P_{ye}. Instead, the brace tensile force was approximately $P_{çre}$. For the braces used in the test, P_{ye} is approximately 54% larger than P_{cre}; this is important because current provisions assume P_{ye} develops at both initial buckling of the braces and after degradation of the compressive strength of the brace. These results show this is not the case when beam yielding occurs, and designing for this condition will results in an unnecessarily large beam. Instead, the load states shown in Fig. 2 are sufficient.

The measured axial forces of the braces at given story drifts were used to establish the unbalanced load on the chevron beam, which is shown in Fig. 12 as a function of each story drift. As noted in Fig. 2, there are two basic considerations in current requirements for SCBF chevron beams. First, the beam must be designed for the braces in the incipient buckling condition, with P_{cre} in both braces (Fig. 2a). This load combination results in a large axial load with relatively small bending and shear demands on the chevron beam. Fig. 12a supports this conclusion. It plots the horizontal force in the beam (derived from strain gage measurements) as a function of story drift. The frame develops $2P_{cre}\cos\theta$ prior to and at buckling. After buckling, this lateral resistance decreases in the compression brace. To design for this condition, a second load case is considered where the tension brace sustains P_{cre} while the force in the compression deteriorates to approximately $0.3P_{cre}$; this load case induces both a vertical and horizontal load on the beam (Fig. 2b). Fig. 12b shows the measured vertical loads on the beam normalized by this second criteria, and it can be seen that, at story drifts of less than 3 or 4%, this downward vertical unbalanced force never exceeds 35% of current requirements. Further at very small deformations, the vertical force may be a small upward force. The first criterion is not significantly reduced by chevron beam yielding, and hence this beam axial force at the point of maximum brace force must be considered in design. However, the unbalanced vertical force is significantly reduced by chevron beam yielding, and reductions in the vertical force used for design are possible.

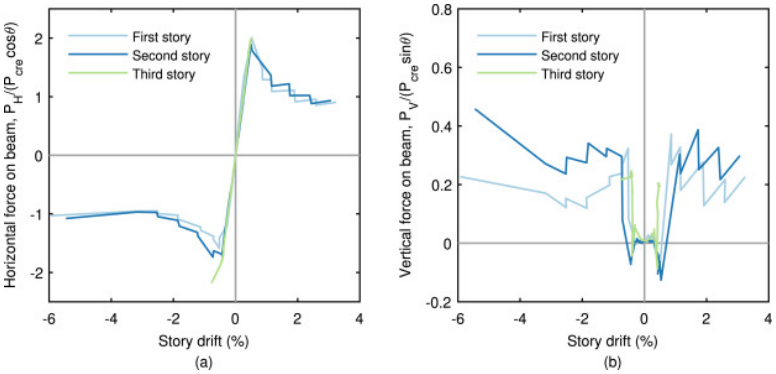

Fig. 12. Measured resultant forces at chevron beam midspan: (a) horizontal and (b) vertical.

2.2.4. Column fracture

As shown in Fig. 9, the test frame experienced unexpected early fracture of the south column at the bottom flange of the second-story beam. The increased strength and stiffness of the top level, a constraint needed for the success of the test, resulted in this fracture. The cause and mitigation of the fracture is investigated using the test data and finite-element analysis modeling, with the latter used to demonstrate that the fracture resulted from the high rotational stiffness of the beam-to-column connections (whereas these connections would likely be simple in a building, since there are no adjacent gusset plates) and the larger stiffness of the beam and composite deck.

The experimental data were used to determine the forces in the column above and below the second-story beam-to-column connection. Note that this connection has flexural stiffness and resistance due to the gusset plate at the bottom of the third story; this resistance is inherent to the configuration and would be present in a building.

Fig. 13 shows the envelope of column shear forces, $V_{col.}$, normalized by the total shear force for each story (i.e., the base shear), V_{base}. Typically, it is assumed that the shear force in the columns and braces resists the applied load. Considering the data in Fig. 13, this is true for the first- and second-story columns but not the third-story columns. Prior to brace buckling, the columns resisted less than 10% of the total lateral force and all the columns sustain shear demands that resist (oppose) the applied shear force. As discussed previously, initial

buckling of the first-story braces occurred at approximately 0.4% story drift, at which the shear forces in the first-story columns increase where the shear forces in the second- and third-story columns decrease (still opposing the applied force). At buckling of the second-story braces, the shear forces in the second-story columns also decreases (again, still opposing the applied force). However, the shear forces in the third-story columns increase at this point; that is, they are in the same direction as the applied load. This has two consequences. First, it increases the forces on the third-story braces since the applied and column shear forces are now additive; by the end of the test, the top-story columns effectively increased the forces on top story braces by approximately 25%. Second the moment demand above and below the second story beam-to-column connection are in the same direction, resulting in almost uniform tension on the front face of the column when the frame is displaced in the positive loading direction. This demand precipitated fracture of the column at this connection.

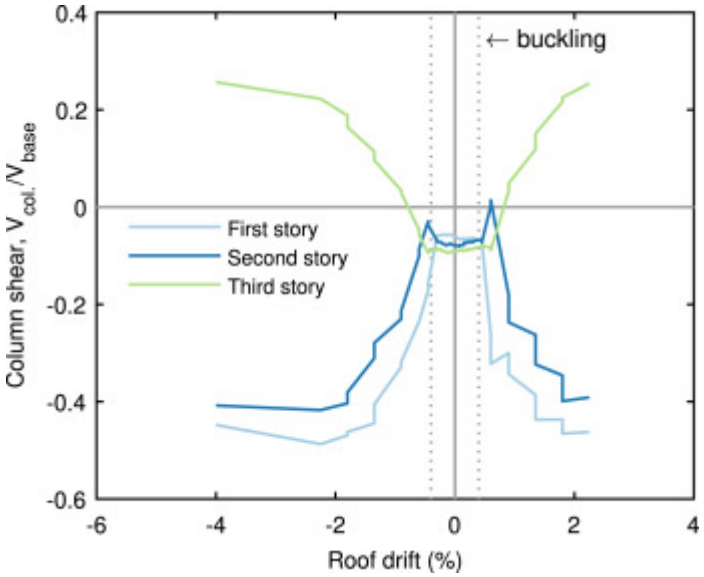

Fig. 13. Shear developed in columns.

3. Computational investigation

To support and further the experimental testing, nonlinear finite-element (FE) analyses were performed using the Abaqus (version 6.14-2) computer program [19] to simulate the response of the test specimen and evaluate the column fracture resulting from the stiffer and stronger top story.

3.1. Finite-element model

Fig. 14 shows the FE model of the three-story test specimen. The model was constructed using four-node, quadrilateral, shell elements with reduced integration (S4R) for all steel components and eight-node, solid elements with reduced integration (C3D8R) for all concrete (i.e., the composite slab). The reinforcing steel in concrete (welded-wire mesh) and corrugated metal deck were not explicitly modeled. A relatively fine mesh (approximately 25 mm by 25 mm) was used in regions where significant inelastic deformation was expected (near beam-to-column connections, gusset-plate connections, and braces); a coarser mesh was used elsewhere.

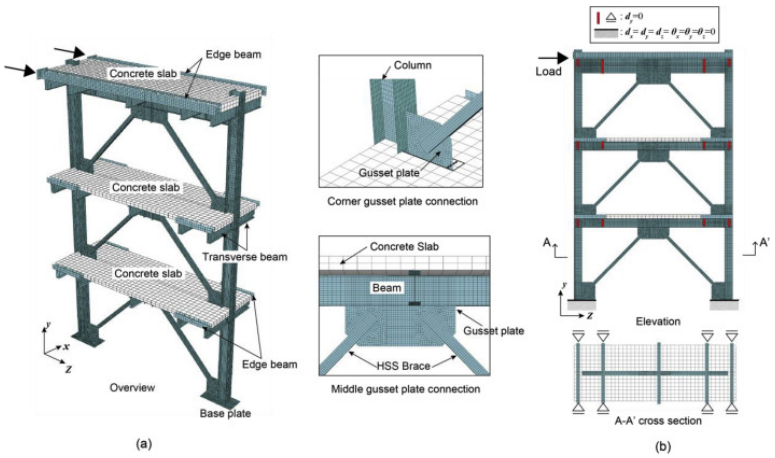

Fig. 14. Analytical model: (a) finite-element mesh and (b) loading and boundary conditions.

The steel and concrete were modeled with a bilinear, kinematic-hardening plastic material model and a concrete damaged plasticity model, respectively. Measured material properties were used. At each level, the steel beam and concrete composite deck were connected at the stud locations to develop partial composite action. The connectors were three-dimensional springs with a rigid-perfectly plastic material response for deformations parallel to the beam axis and rigid for other translations and rotations. The horizontal spring resistance was determined from the shear-stud strength in ANSI/AISC 360-16 [23]. Similar connectors were placed at the locations of the shear studs connecting the slab edge beams to the concrete in the composite deck.

The model was subjected to the cyclic drift history shown in Fig. 5. The same displacements were imposed at the end of third-story edge beams where the actuators were attached in the experimental setup (shown in the photograph in Fig. 3a). The bottoms of the column base plates were fully restrained, and the ends of transverse beams adjacent to the beam-to-column connections were restrained against OOP movement and rotation.

A large-displacement formulation was used to simulate member geometric nonlinearity and buckling. Initial geometric imperfections were used based on eigenvalue buckling analyses of the frames with horizontal load. The magnitudes of imperfections were determined so that the sequence and direction of buckling of braces matched those observed in the test. Specifically, the maximum out-of-straightness was 1/500 of the brace length for the second- and third-story braces and 1/333 of the brace length for first-story braces.

Cyclic inelastic analyses were completed for the test frame up to the drift at which column fracture occurred for three models. The three models varied as follows:

1. Model AB simulated the as-built condition with composite slabs on all levels and fully restrained beam-to-column connections.
2. Model SC was identical to Model AB except that the top-story beam-to-column connections were modeled as simple connections in order to explore the impact of the flexural stiffness of the top story on the column fracture the frame sustained during the test and to investigate if this is a concern for more realistic applications.
3. Model BB was identical to Model AB except that the slabs on the bottom two levels were removed. The Model AB and BB analyses bounded the experimental results, since the composite deck separated from the first- and second-story beams at large deformations in the test, as shown in Fig. 8d.

3.2. Model validation

Fig. 15 compares the experimentally measured and computationally simulated shear-versus-story drift responses for Models AB and BB. Both models captured the deformation distribution reasonably well, but discrepancies in the experimental and computational story drifts occurred because the real-time evolution of story stiffness and strength due to composite-action deterioration in the beams was not simulated. The following paragraphs discuss how these models bound the actual response and confirm the detrimental effects of the stiff and strong top story.

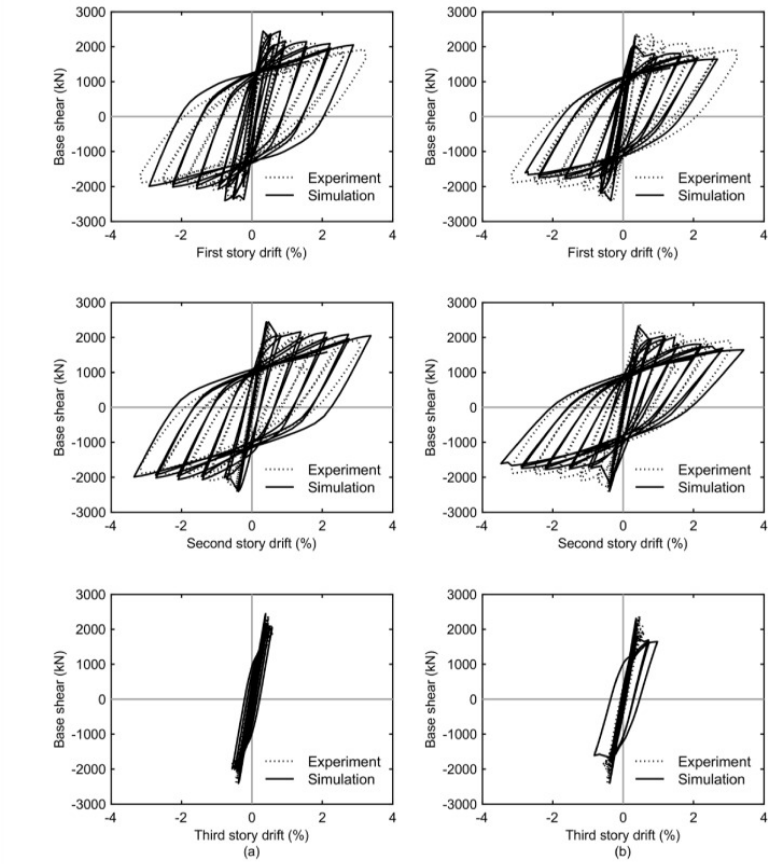

Fig. 15. Computed results: (a) Model AB (with slab) and (b) Model BB (without slab).

3.2.1. Validation of model AB

At story drifts exceeding approximately 2%, Model AB captures the resistance; the resistance is overpredicted by less than 10% for larger drift demands. To further validate the model, the locally deformed shape and extent of yielding (observed by flaking of whitewash) are compared with the deformed shape and stress contours in Fig. 16. This figure compares the second-story gusset plates, first-story columns, and first-story beam. The results demonstrate that the model is capable of modeling the full nonlinear (material and geometric) response of the system. There is quite good comparison between the predicted and observed deformations, and the equivalent plastic strain contours suggest good agreement between the predicted and observed locations and extent of local buckling and yielding. These results combined with the force-drift response hystereses shown in Fig. 15 validate the modeling approach. This model will be used in the remainder of the paper, with changes in member properties, connections, and slab (i.e., included or not) to investigate their impact on response.

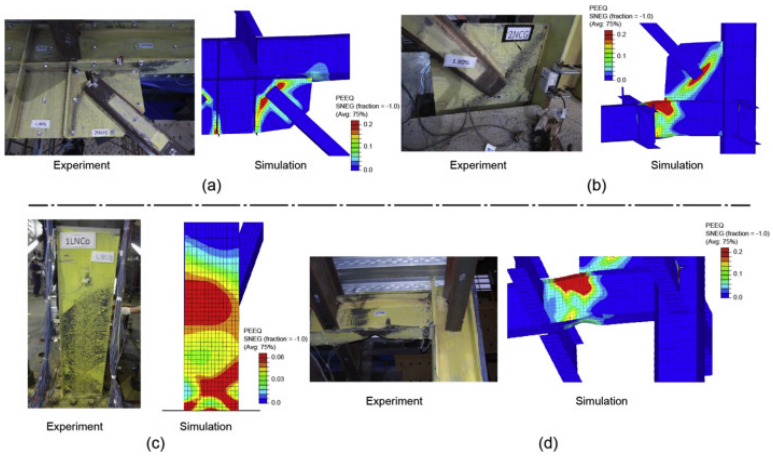

Fig. 16. Measured and simulated (Model AB) damage states observed at 1.8% roof drift: (a) middle gusset plate at the second story; (b) corner gusset plate at the second story; (c) column flange at first story; and (d) north beam end at the first story.

3.2.2. Comparison to model SC

The first modification made to the model was to use a single-plate shear beam-to-column connection, rather than fully restrained connection, at the top level. In the test, the column flange fractured at approximately 3% story drift in the second story. The nonlinear computer models do not attempt to predict fracture, but examination of the state of stress at this connection and deformation level aids in understanding the observed behavior. Fig. 17 compares the computed vertical and hydrostatic stress states at approximately 3% drift for Models AB (as-built condition) and SC (simple connection). For Model AB, the inner flange and web of the south column sustain significant vertical tensile stress throughout the height of the second-story beam-to-column connection. This stress distribution results from the approximately constant (same direction) moments induced above and below the connection due to the reversal of column shear forces in the second and third stories (see Fig. 11). These stresses are not present in Model SC because of the reduced flexural resistance and stiffness of the third-story beam-column connection; here, the column load reversal does not occur. In addition to vertical stresses, it is of interest to study the hydrostatic stresses. Large hydrostatic tensile stresses are known to induce fracture, with the hydrostatic stress defined through the first-principle invariant of the stress state. It can be seen that large hydrostatic tensile stresses develop in Model AB (Fig. 17c) in the column web and flange adjacent to the beam bottom-flange weld, with a local maximum near the center of the beam and column web at this welded joint, where fracture initiated in the test. In comparison, these large stresses are not present at this location in Model SC (Fig. 17d). Since the vast majority of chevron-configured SCBFs would use simple beam-column connections at locations without a gusset plate, the column fracture sustained in the test is clearly a result of the boundary conditions and hence unlikely to occur in an actual building.

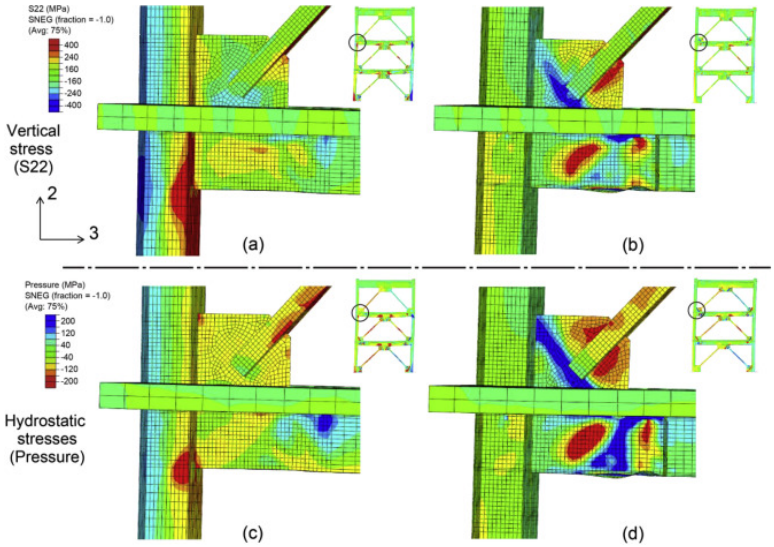

Fig. 17. Computed Vertical (a and b) and Hydrostatic Stress (c and d) at the Fractured Column in the Second-Story Connection. Figures on the left (a and c) for Model AB; Figures on the right (b and d) for Model SC.

3.2.3. Comparison to model BB

As indicated in the test photographs, the composite deck separated from the beam, and hence Model AB is less representative of the test specimen at large deformations. To bound the behavior of the fully connected, partially composite beam and the system without the slab, Models AB and BB (bare beam) were compared. Fig. 15b shows the results of the Model BB analysis. Both models accurately predicted the inelastic deformation of the second story and both models underestimated the inelastic deformation in the bottom story. The measured chevron beam deflections were 42% larger than the computed values from the composite model (AB), but the bare-steel model (BB) estimated these beam deflections well with a maximum error of about 5%. The OOP deformations of the braces were predicted with reasonable accuracy by both models.

From the comparison of the numerical and experimental results above, it is clear that the two models bound the true behavior. Model AB simulates the experimental response best until about 2% story drift, when composite action began to deteriorate in the test but not in the model. After this stage, Model BB is most representative of the experimental response and thus is a better predictor of the ultimate behavior. Model BB, with bare-steel beams for the bottom two stories, was used in the computational parametric study described below to examine different beam strengths for two reasons: (1) the strength of the beam under combined loading is known and is not dependent upon load state or history as in the case of a composite beam, which is critical to determining a final design expression and (2) the model provides a more accurate estimate of the strength after deck delamination.

3.2.4. Parameter study of beam strength

The single-story tests of chevron SCBFs with yielding beams [10] and the three-story test described here showed that yielding chevron beams can increase drift capacity of SCBFs. In part, this is because the tensile brace force is limited due to beam yielding. At the initiation of brace buckling, the forces in both the compression and tension braces are equal to P_{cre} regardless of the beam strength. After buckling, the force in the compressive brace deteriorates; the test results indicate that a lower bound of $0.3P_{cre}$ is appropriate, and this is consistent with current practice [3]. These observations lead to two load states, as shown in Fig. 2. In the first (elastic) load state, both the tensile and compressive braces attain P_{cre}. The second load state is capacity based with respect to the beam and combines a tensile brace force with magnitude of P_{cre} in tension and a deteriorated compressive brace force of $0.3P_{cre}$ in compression. The three-story test specimen was designed to sustain this

second load state while permitting beam yielding. In addition, the flexural resistances of the specimen's beams were evaluated assuming partial composite action with the slab. Using the results shown in Fig. 15, a small parametric study was conducted based on Model BB to investigate the impact of beam sizes and evaluate the proposed dual-load state design, shown in Fig. 2.

Four variations in the beams at the first and second levels of the three-story model were considered. These had strengths of 69%, 114%, 147% and 179% of the beam strength required to meet the demand illustrated in Fig. 2b. The weakest beam corresponded to the W14 × 30 used in the test frame. Note that the beam flexural strength was computed assuming a plastic collapse mechanism where plastic hinges form at the gusset plate edges and the axial strength was taken as the product of the yield stress and gross area, which assumes it is fully braced for compression. Additionally, the axial load demand in the beam for both states in Fig. 2 was assumed to be equally distributed between the two ends of the beams. All beams evaluated had sufficient axial strength to develop the demands illustrated in Fig. 2a.

Fig. 18 plots the predicted lateral resistance as a function of roof drift for the four simulations using different beam sizes. To demonstrate acceptable response, the frames are expected to develop a maximum resistance of at least $2P_{cre}\cos\theta$, as expected at incipient brace buckling, and sustain a resistance of at least $2P_{crn}\cos\theta$, the design resistance, up to a story drift of 2%. Fig. 18a shows a chevron SCBF with a beam that has 69% of the proposed minimum resistance; as noted in the plot, there is significant deterioration in lateral strength that increases with large inelastic deformation levels. In Fig. 18b, the SCBF had a beam with 114% of the proposed minimum strength; this frame has nearly identical maximum lateral resistance to the test frame, sustained a slight loss in resistance at brace buckling, and retained this resistance without deterioration (i.e., meeting the acceptance criteria above). Fig. 18c and d shows the results for SCBFs with stronger beams; however, these frames only had 20% larger resistance than the weakest beam (Fig. 18a) considered. Although the lateral resistance was stable following brace buckling, tests have shown that the braces of these frames would fracture at much smaller story drifts because of the cyclic tensile and compressive strain demands. In all cases, it is noted that these analyses underestimate the resistance and overestimate the deterioration because the strengthening effect of the slab is neglected.

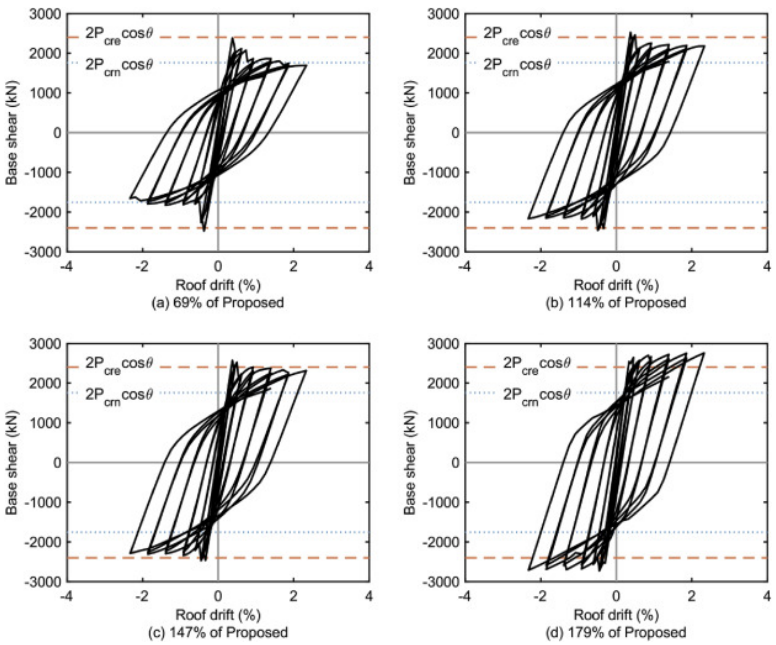

Fig. 18. Comparison of computed behavior as a function of chevron beam resistance.

In addition to strength and deformability, vertical deflection of beams in chevron configured SCBFs are a concern. Fig. 19 shows the computed beam deflections for the bottom-story beam from four of the analyses with different beam sizes. As expected, the beam deflection increases with a reduction in beam resistance, but this relationship is not linear. At 2.5% drift, the predicted deflection of the beam with 69% of the proposed unbalanced load resistance was approximately 75 mm (3 in.) compared to approximately 80 mm (3.2 in) measured deflection in the test. The deflection of the beam with 114% of the proposed minimum resistance was approximately 60 mm (2.4 in.). The model with a beam having 179% of the proposed resistance approximates current SCBF requirements and it has approximately 32 mm (1.3 in.) deflection.

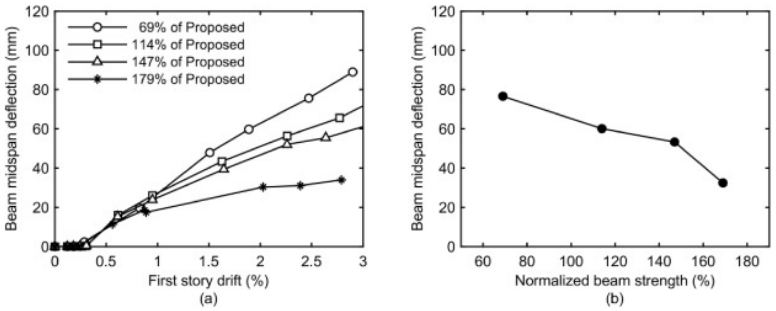

Fig. 19. Computed beam deflection: (a) beam midspan deflection versus story drift; (b) beam midspan deflection at 2.5% story drift versus normalized strength.

Proper design of beams in chevron configured frames requires accurate estimate and distribution of vertical forces (which determine the moment demand) and horizontal forces (which determine the axial demand). Fig. 20a plots the computed vertical force, normalized by $P_{cre}\sin\theta$, on the chevron beam as a function of beam strength and story drift. The force becomes larger for stronger beams. However, the vertical force never reaches the current design limit, $(P_{ye} - 0.3P_{cre})\sin\theta$, even with a beam that remains elastic; this is due in part to elastic deflection of the beam.

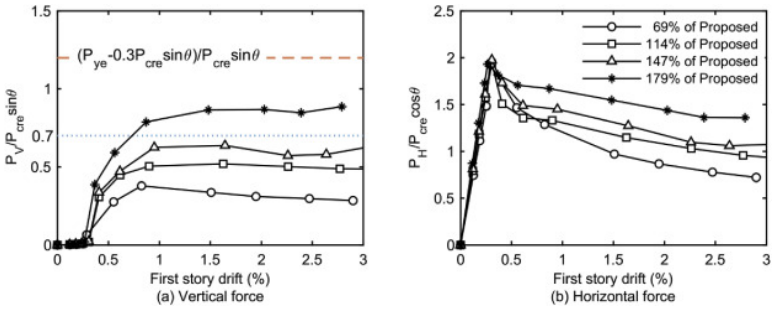

Fig. 20. Comparison of computed beam force to proposed design model.

The horizontal force on the beam is equally important, as the beam must be designed for combined loading. Fig. 19b shows the horizontal force calculated from the analysis; the force results from the braces and, as expected, is a function of beam resistance and story drift. The horizontal force equals $2P_{cre}\cos\theta$ for all beam strengths at the brace buckling deformation, which corresponds to the state depicted in Fig. 2a. It reduces to $1.3P_{cre}\cos\theta$ for the second load case. These results, combined with the experimental results, are described further in the next section.

3.2.5. Proposed design expressions for unbalanced force

The experimental and analytical results were combined to propose a revised capacity-based expression for the design of beams with permitted yielding in chevron SCBFs. The expression, shown in Fig. 2b, modifies the

maximum tensile force of the brace to be equal in magnitude to P_{cre} of the brace at incipient buckling (Load State 1, Fig. 2a) *and* at large deformations after buckling, where the compressive brace force has degraded (Load State 2, Fig. 2b). The research also shows that $0.3P_{cre}$ is an appropriate limit for the deteriorated strength of the compressive brace. As a result, the proposed design procedure continues to require two separate design load states. The analytical and experimental research on single-story [10] and three-story chevron SCBFs demonstrates that this design procedure will result in stable lateral resistance with no significant deterioration of resistance until brace fracture. Further, the yield deformation of the beam will result in increased inelastic deformation capacity of the brace and brace frame prior to brace fracture.

Although the composite slab does contribute resistance, it is recommended that the bare steel beam be designed for these applied loads. Tests show that the vertical beam deformations that occur cause deterioration of this partial composite resistance at large drifts (2% or greater). The chevron beam should be designed for the combined bending moments and axial loads by the requirements of Chapter H of the AISC *Specification* [23]. For determination of the axial loads and moments with the deteriorated compressive brace, the geometries shown in Fig. 21 may be employed. Fig. 21a applies to beams with corner gusset plates, where the column is strong enough to develop the plastic bending capacity of the beam (a third design requirement for these systems). Yielding of the beam adjacent to the gusset plate is justified by experimental research which has shown that corner gusset-plate connections provide significant end rotational restraint to the beam. Fig. 21b applies to beams where corner gusset plates are not present and simple shear-tab connections are employed (e.g., single-story chevrons and the top story of multistory chevrons). Flexural demand for beam, M_r for the beams with and without corner gusset plates are derived from assumed collapse mechanisms using the virtual work equation and can be expressed by following equations:(1)Mr=PV8(L−Lmp−2Lcp−dc)=PVl14(2)Mr=PV4(L−Lmp−dc)=PVl22where l_1 and l_2 are clear length between rigid links.

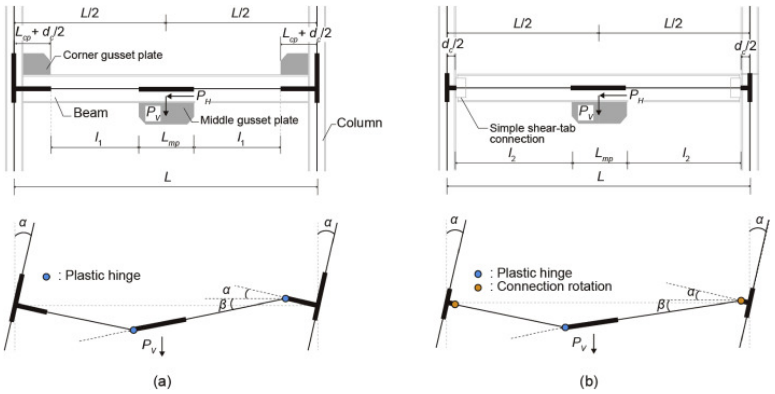

Fig. 21. Determination of moments and axial forces in chevron beam: (a) with corner gusset plates and (b) without corner gusset plates.

4. Summary and conclusions

This paper presents research on the nonlinear behavior of multistory chevron SCBFs with yielding beams and is a complementary study to a prior research phase focusing on single-story chevron SCBFs. The research is founded on an experimental investigation of a three-story SCBF with yielding chevron beams subjected to significant inelastic drift demands which would be expected in large earthquakes. The beams were designed by the design strategy presented in this paper (Fig. 2b) with the beam resistance evaluated considering the partial composite resistance of the beam. The test was performed at the NCREE Laboratory in Taipei, Taiwan. The frame exhibited good inelastic behavior. There was no brace fracture despite achieving story drifts exceeding 5% and story-drift ranges greater than 8%. However, separation of the steel beams and composite slabs were observed at larger drifts, which led to an undesirable deterioration in the lateral resistance.

Nonlinear finite-element analyses were performed in support of and to extend the experimental research. Two different models were considered and compared to the experimental results: one with a composite deck and one without. The results bounded the test results. The bare-beam model (Model BB, without a composite deck) was used to conduct a limited parametric study to investigate the impact of beam strength on cyclic response. The results show that yielding beams that meet the proposed load cases have sufficient strength to resist the design lateral loads and do not sustain significant deterioration in strength. Combined with the test results for the one-story frames, the research also has demonstrated that chevron SCBFs with yielding beams have more drift capacity prior to brace fracture.

The results of the one-story and three-story experimental and analytical results demonstrate a new, robust system with large inelastic deformation capacity prior to initial brace fracture. In particular, the results show that:

- Multistory chevron SCBFs are capable of ductile behavior and are not necessarily susceptible to early, soft-story failure modes. However, the result observed in the multistory test was, in part, a function of the top-story location and imposed symmetric history of the applied load. The chevron beams were designed to the proposed resistance level from this research including the partial composite resistance of the beam. The three-story test frame developed its full expected resistance and achieved story drifts of 5.9% and 5.4% in the first and second stories, respectively, with no brace fracture. These deformations corresponded to drift ranges of 9% and 8.6% in the first and second stories, respectively.
- At large drifts, there can be separation of the steel beam and the composite slab. In the test, this resulted in moderate deterioration in resistance since the bare steel beam was weaker than the composite beam. Based on these results, it is proposed that composite action be neglected in computing the strength of beams in chevron SCBFs.
- The unusually stiff and strong top story of the test specimen resulted in large stress demand at the top of the second story column which precipitated fracture. Computational modeling showed that these demands would be alleviated if the top-story beam had simple connections, as is typical. Large differences in beam strength relative to the braces from story to story should be avoided.
- Beam yielding limits the demand in the tension brace and therefore the unbalanced load on the beam. Two load states on the beam must be considered. At brace buckling, the beam is subject to the horizontal load equal to $2P_{cre}\cos\theta$, regardless of its strength. At advanced deterioration of the strength of the compressive brace, the vertical unbalanced load is $0.7P_{cre}\sin\theta$ and the total horizontal load is $1.3P_{cre}\cos\theta$, which is assumed to be equally distributed in tension and compression to the beam. This load state in shown in Fig. 2b.
- A parameter study using high-resolution finite-element models investigated the effect of various beam strengths on the inelastic performance of chevron SCBFs with yielding beams. It was shown that the current unbalanced load condition produced by tensile braces at P_{ye} and compressive braces at P_{cre} is not achieved even with very strong beams that remain elastic. Beam deflection and/or yielding controls the magnitude of this unbalanced force. Hence, designing for a large unbalanced load results in a large unbalanced load, but the corresponding inelastic behavior may be less desirable than provided by a yielding (weaker) beam.

This research has further illustrated the benefits of chevron beam yielding on global inelastic behavior and its potential use in seismic design. The work led to a design method, and this study and prior research [10] shows that this method significantly reduces the beam size required for chevron SCBFs while increasing the inelastic deformation which can be sustained prior to brace fracture. This behavior has been documented through experiments and nonlinear analysis of single-story and three-story frames. However, additional work is needed

(and ongoing) to document system performance and seismic (i.e., dynamic) response for a wider range of parameters including number of stories, brace slenderness, and frame geometry.

Acknowledgments

This research was funded by the American Institute of Steel Construction. Mr. Tom Schlafly was the program manager for this work. James Malley, Rafael Sabelli, and Tom Sabol served as technical advisors to the research team. The numerical analyses were conducted with partial financial support provided by the Japan Society for the Promotion of Science under Grant No. R2904. The financial support from these agencies and all technical advice is greatly appreciated and gratefully acknowledged.

References

[1] ICBO. **Uniform Building Code.** International Conference of Building Officials, Whittier, CA (1988)

[2] AISC. **Seismic provisions for structural steel buildings.** ANSI/AISC 341-97, American Institute of Steel Construction, Chicago, IL (1997)

[3] AISC. **Seismic provisions for structural steel buildings.** ANSI/AISC 341-16, American Institute of Steel Construction, Chicago, IL (2017)

[4] D.A. Foutch, S.C. Goel, C.W. Roeder. **Seismic testing of full-scale steel building—Part I.** J. Struct. Eng., 113 (1987), pp. 2111-2129, 10.1061/(ASCE)0733-94451987)113:11(2111

[5] T. Fukuta, I. Nishiyama, H. Yamanouchi, B. Kato. **Seismic performance of steel frames with inverted V braces.** J. Struct. Eng., 115 (1989), pp. 2016-2028, 10.1061/(ASCE)0733-9445(1989)115:8(2016)

[6] C.W. Roeder. **Seismic behavior of concentrically braced frame.** J. Struct. Eng., 115 (1989), pp. 1837-1856, 10.1061/(ASCE)0733-94451989)115:8(1837

[7] A.D. Sen, C.W. Roeder, J.W. Berman, D.E. Lehman, C.-H. Li, A.-C. Wu, K.-C. Tsai. **Experimental investigation of chevron concentrically braced frames with yielding beams.** J. Struct. Eng., 142 (2016), Article 04016123, 10.1061/(ASCE)ST.1943-541X.0001597

[8] B.G. Simpson, S.A. Mahin. **Experimental and numerical evaluation of older chevron concentrically braced frames with hollow and concrete-filled braces.** J. Struct. Eng., 144 (2018), Article 04018007, 10.1061/(ASCE)ST.1943-541X.0001988

[9] C.R. Bradley, L.A. Fahnestock, E.M. Hines, J.G. Sizemore. **Full-scale cyclic testing of low-ductility concentrically braced frames.** J. Struct. Eng., 143 (2017), Article 04017029, 10.1061/(ASCE)ST.1943-541X.0001760

[10] C.W. Roeder, A.D. Sen, C. Terpstra, S.M. Ibarra, R. Liu, D.E. Lehman, J.W. Berman. **Effect of beam yielding on chevron braced frames.** J. Constr. Steel Res., 159 (2019), 10.1016/j.jcsr.2019.04.044

[11] M. D'Aniello, S. Costanzo, R. Landolfo. **The influence of beam stiffness on seismic response of chevron concentric bracings.** J. Constr. Steel Res., 112 (2015), pp. 305-324, 10.1016/j.jcsr.2015.05.021

[12] I.F. Khatib, S.A. Mahin, K.S. Pister. **Seismic behavior of concentrically braced steel frames.** UCB/EERC-88/01, Earthquake Engineering Reserach Center, Berkeley, CA (1988)

[13] T. Okazaki, D.G. Lignos, T. Hikino, K. Kajiwara. **Dynamic response of a chevron concentrically braced frame.** J. Struct. Eng., 139 (2013), pp. 515-525, 10.1061/(ASCE)ST.1943-541X.0000679

[14] R. Tremblay, N. Robert. **Seismic performance of low- and medium-rise chevron braced steel frames.** Can. J. Civ. Eng., 28 (2001), pp. 699-714, 10.1139/l01-038

[15] Y. Balazadeh-Minouei, S. Koboevic, R. Tremblay. **Seismic assessment of existing steel chevron braced frames.** J. Struct. Eng., 144 (2018), Article 04018046, 10.1061/(ASCE)ST.1943-541X.0002037

[16] E.J. Lumpkin, P.-C. Hsiao, C.W. Roeder, D.E. Lehman, C.-Y. Tsai, A.-C. Wu, C.-Y. Wei, K.-C. Tsai. **Investigation of the seismic response of three-story special concentrically braced frames.** J. Constr. Steel Res., 77 (2012), pp. 131-144, 10.1016/j.jcsr.2012.04.003

[17] C.W. Roeder, E.J. Lumpkin, D.E. Lehman. **A balanced design procedure for special concentrically braced frame connections.** J. Constr. Steel Res., 67 (2011), pp. 1760-1772, 10.1016/j.jcsr.2011.04.016

[18] A.D. Sen, M.A. Swatosh, R. Ballard, D. Sloat, M.M. Johnson, C.W. Roeder, D.E. Lehman, J.W. Berman. **Development and evaluation of seismic retrofit alternatives for older concentrically braced frames.** J. Struct. Eng., 143 (2017), Article 04016232, 10.1061/(ASCE)ST.1943-541X.0001738

[19] Dassault Systemes, Abaqus Unified FEA, (2014).

[20] ATC. **Guidelines for cyclic seismic testing of components of steel structures for buildings.** Rep. ATC-24, Applied Technology Council, Redwood City, CA (1992)

[21] S.M. Ibarra. **Experimental Investigation of Chevron Special Concentrically Braced Frames with a Yielding Beam Plastic Mechanism.** University of Washington (2018)

[22] C.W. Roeder, D.E. Lehman, J.W. Berman, S.M. Ibarra, C. Terpstra, A.D. Sen, T. Li, R. Liu. **Investigation of Chevron-Configured Special Concentrically Braced Frames: A Report to the** American Institute of Steel Construction, Seattle, WA (2017)

[23] AISC. **Specification for structural steel buildings.** ANSI/AISC 360-16, American Institute of Steel Construction, Chicago, IL (2017)